

Lane and band formation of oppositely driven colloidal particles in two-dimensional ring geometries

Tobias Vater , Marc Isele , Ullrich Siems, and Peter Nielaba ^{*}
Physics Department, University of Konstanz, 78467 Konstanz, Germany



(Received 8 April 2022; accepted 18 July 2022; published 8 August 2022)

We study the segregation phenomena for oppositely driven colloidal particles in two-dimensional ring geometries by means of Brownian dynamics simulations without hydrodynamic interactions. The particles interact via a repulsive Yukawa potential and are confined to a two-dimensional circular channel by hard walls, in which half of the particles are driven clockwise and the other half are driven counterclockwise. In addition to lane formation, which is commonly found in oppositely driven systems, we found band formation along the angular direction in channels with a very large radius. This indicates that a formation of lanes is prevented in the limit of channels with an infinitely large inner radius. The dependency of this segregation has been examined for the two control parameters, the interaction strength between the particles and the width of the circular channel.

DOI: [10.1103/PhysRevE.106.024606](https://doi.org/10.1103/PhysRevE.106.024606)

I. INTRODUCTION

Colloidal systems in restricted microchannels [1–5] are good model systems for the understanding of systems on different length scales like atomic wires [6,7], lab-on-a-chip devices [8,9], or the behavior of ants [10] despite their diversity and complexity. Colloidal model systems are an important approach to analyze and find dynamical phenomena [11–18] in systems far from thermodynamic equilibrium. Thus it is very interesting to study these systems for nonequilibrium order phenomena which arise for different system sizes and parameters.

For oppositely driven colloidal particles moving according to Brownian motion, global lane formation for two- and three-dimensional systems was found [19,20]. Similar behavior was found in systems of pedestrians [21–23], which also show lane formation. Local lane formation was also found in experiments of oppositely charged colloids in an electric field [24,25] as well as in an alternating electric field [26] or in binary plasma [27]. In addition, phase diagrams of oppositely charged particles in an electric field calculated in terms of Brownian dynamics simulations [28] and the influence of the hydrodynamic interaction [29] was investigated.

Recent publications [30] questioned whether lane formation in two-dimensional systems is a real transition in the sense that it survives in the thermodynamic limit of an infinitely long channel or if it is only a finite-size effect supported by the periodic boundary condition. The systems we examined in this work do not possess periodic boundary conditions but rather an inherent periodicity that lies within their circular shape. Since an experimental circular channel setup is conceivable, this periodicity is not an artificial numerical boundary condition, but a very real component and leads therefore to fewer artifacts.

In the case of particles driven oppositely by oscillating external fields for certain sets of parameters a formation of bands orthogonal to the driving direction could be found as well [26,31]. Such bands are the result of two particle fronts that span the whole width of the channel colliding and then passing through each other. Such a demixing along the driving direction has also been found in simulations of three-dimensional channels with a constant driving force [13]. A similar formation of bands is also known from the Viscek model, which is a simple model for anisotropic self-propelled particles [32]. The so-called flocking transition occurs as a function of density or noise in large systems [33,34]. It describes the formation of bands of self-propelled particles moving collectively along the direction orthogonal to the band.

In our work, we deal with the question whether these ordering phenomena can be found in two-dimensional circular channels and how they depend on various parameters like radius, width, and potential strength. The influence of hydrodynamic interactions has been neglected in this study, even though it has been shown to slightly modify the ordering phenomena in similar studies [29,35]. In particular, study of band formation in oscillating fields [35] reveals that the band formation is blurred by including hydrodynamic interactions. However, the system without hydrodynamic interactions is an important simplified model, since they strongly depend on the experimental realization, especially in two dimensions. They are different when the particles are either aggregated in a monolayer within a three-dimensional bulk fluid, assembled close to a fluid interface, or even confined between two parallel plates [36]. This lane formation and the band formation are not unique to colloidal system; in fact, they also occur in systems where no hydrodynamic interaction is present.

This paper is organized as follows. Section II describes the model, which shows how the simulations are set up. In Sec. III the two order parameters that give numerical statements about lane and band formation are explained. These order parameters are used to quantify the observed phenomena and compare different systems. Section IV presents the

^{*}peter.nielaba@uni-konstanz.de

results from the simulations, how the systems arrange with increasing driving forces, when lane formation occurs, and what happens when the width of the system changes. It also demonstrates in which parameter space the formation of bands of particles perpendicular to the driving force occurs. In Sec. V the results are summarized.

II. MODEL

In this study, the motion of colloids is modeled by Brownian dynamics simulations in two dimensions, where the hydrodynamic interactions are neglected. This can be described by a stochastic Euler integration of the overdamped Langevin equation. The positions of the particles are updated according to [37] with

$$\mathbf{r}_i(t + \Delta t) = \mathbf{r}_i(t) + \frac{D_0 \Delta t}{kT} \mathbf{F}[r_j(t)] + \sqrt{2D_0 \Delta t} \mathbf{R}(t), \quad (1)$$

where Δt is the time step, kT is the unit of the thermal energy, D_0 is a microscopic diffusion constant, and $\mathbf{F}[r_j(t)]$ is the driving force. $\mathbf{R}(t)$ consists of Gaussian random numbers that are defined by the properties $\langle R_i(t) \rangle = 0$ and $\langle R_i(t) R_j(t) \rangle = \delta_{ij}$. The starting positions of the particles in the simulation are randomly distributed throughout the channel, respecting a minimum mutual distance of σ .

The particles interact via the Yukawa potential

$$V(r_{ij}) = \begin{cases} V_0 \frac{\exp(-\kappa r_{ij})}{r_{ij}} & : r_{ij} \leq r_c \\ 0 & : r_{ij} > r_c \end{cases}, \quad (2)$$

where κ is the inverse screening length, V_0 is the interaction strength, and r_{ij} is the distance between two particles. To reduce the computational effort, a cutoff radius of $r_c = 3.0\sigma$ is introduced. The potential is continuous up to the cutoff radius.

The particles are confined to a ring geometry, which is defined by its boundary consisting of two concentric circles with an inner radius R_1 and an outer radius R_2 . Compared to a linear channel this circular geometry has the advantage that periodic boundary conditions in a tangential direction are implemented naturally. With such a system counterflow can be realized in experiments as shown in Ref. [38]. The boundaries in the simulations are realized as hard walls analogously to Ref. [39]. Different system sizes were investigated by simulations at a constant particle density $n = \frac{N}{A}$, where N is the number of particles and $A = \pi(R_2^2 - R_1^2)$ the area of the ring.

There is an external force which drives one half of the particles in the clockwise direction, and a further external force which drives the other half of the particles in the counterclockwise direction. These forces on the particles are described by

$$\mathbf{F}_i = (-1)^i \cdot \begin{pmatrix} -y_i \\ x_i \end{pmatrix} \cdot \frac{F}{R_1}, \quad (3)$$

acting on the i th particle depending on its position $\mathbf{r}_i = (x_i, y_i)$, the inner radius R_1 of the system, and the absolute value of the force F . The direction of motion is opposite for even and odd particle indices. The value of the driving force is highest at the outer edge while decreasing inwards, in a way that all particles have the same absolute angular velocity $\omega = F/R_1$. This has the advantage that each particle has the

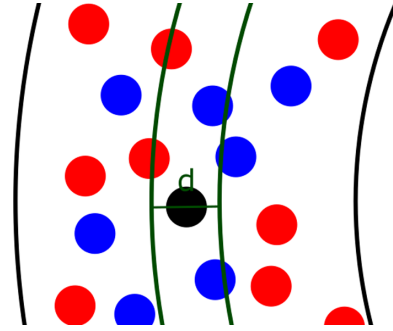


FIG. 1. Schematic representation of the radial tube around a particle i inside of which all particles j contribute to the lane formation parameter. Particle i and the channel wall are represented in black, the small tube around i and the width d of the tube are displayed in green.

same orbital period, which results in there being no internal shear between particles of the same parity.

This model has five independent control parameters: V_0 and κ from the interaction, inner radius R_1 , the channel width $W = R_2 - R_1$, and the external force F .

III. OBSERVABLES

To get accurate statements regarding the order in the systems, two order parameters Φ_{lane} and Φ_{band} are introduced. These parameters represent a numerical value of the two different ordering states. In the following we consider two particle species which differ only by the direction in which they are driven.

A. Order parameter for lane formation

The lane formation parameter is similar to the description of the ordering in a linear system [13]. Here it describes the radial segregation of the two particle species. Particles of the same species having a similar radial coordinate $\rho_i = \sqrt{x_i^2 + y_i^2}$ are considered as moving in a lane.

For each particle i a radial tube of width $d = 1.5\sigma$ is considered. All the other particles that lie in the tube contribute to the order parameter of the i th particle. In other words, each particle j within this radial distance $\rho_{ij} < d/2$ contributes to the order parameter of the i th particle. A schematic of this tube can be seen in Fig. 1. Subsequently the radial distances in the xy plane between particle i and j are determined by

$$\rho_{ij} = \rho_i - \rho_j. \quad (4)$$

For all particles j inside the neighborhood of particle i , either $N_{i,+}$ is incremented by one if the particles are of the same type or otherwise $N_{i,-}$ is incremented by one. In addition, it is defined that $n_{i,+} = |N_{i,+}|$ and $n_{i,-} = |N_{i,-}|$. The order parameter for lane formation is calculated by

$$\Phi_{l,i} = \frac{n_{i,+} - n_{i,-}}{n_{i,+} + n_{i,-}}, \quad (5)$$

$$\Phi_{\text{lane}} = \frac{1}{N} \sum_{i=1}^N \Phi_{l,i}, \quad (6)$$

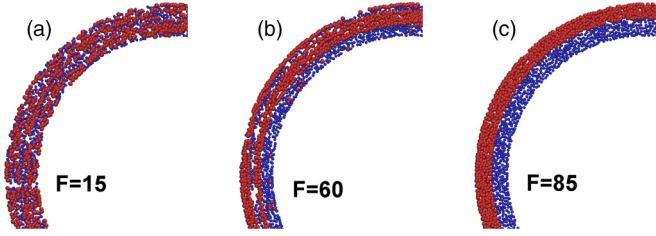


FIG. 2. Snapshot of the circular channel with radius $R_1 = 90$ and width $W = 20$ with different driving forces. The picture on the far left (a) shows the system with a driving force of $F = 15$, in this case there is disorder. Panel (b) shows the system with a driving force of $F = 60$ in the critical area. In this area, the system starts to organize itself. The image on the far right (c) was taken at a force of $F = 85$. The particles separate completely into two lanes. The red particles run in the clockwise direction, the blue particles run counterclockwise.

where $\Phi_{l,i}$ is the order parameter of the i th particle and Φ_{lane} is the global order parameter which is averaged over all N particles. The value of Φ_{lane} is zero if the particles are mixed, and it approaches unity if the particles are radially segregated. In order to visualize the two particle species, they are color coded in red and blue in Fig. 2. The critical force for lane formation $F_{c,\text{lane}}$ is defined as the force where the order parameter reaches a value of $\Phi_{\text{lane}} = 0.5$.

B. Order parameter for band formation

The band formation is a separation phenomenon where the two particle species order in tangential direction. The band order parameter Φ_{band} is determined by the average value of a histogram over the angular positions φ of the particle. The histogram is calculated with $n_{\text{bin}} = 72$ bins in the interval $\varphi \in [0^\circ, 360^\circ]$ and with a bin size of $\Delta\varphi = 5^\circ$. The histogram shows the particle number over the angular coordinate φ , which is calculated for the two particle species separately. This is shown in Sec. IV E.

To calculate Φ_{band} the variance is divided by the squared mean M of the number of particles N in each bin:

$$M = \frac{N}{n_{\text{bin}}}. \quad (7)$$

The variance is obtained from the sum of the mean square deviation of the results around their mean, where n_i is the number of particles in the respective bin:

$$S^2 = \sum_{i=1}^{n_{\text{bin}}} \frac{(n_i - M)^2}{n_{\text{bin}}}. \quad (8)$$

To get a reasonable value for the ordering parameter we divide the variance by the squared mean value

$$\Phi_{\text{band}} = \frac{S^2}{M^2}. \quad (9)$$

If the particles of the same species are equally distributed along the tangential direction, the variance S^2 and thus Φ_{band} is zero. The value of the band order parameter can be greater than unity. The value of $\Phi_{\text{band}} = 1$ corresponds to a scenario where half of the channel is empty, and in the other half of

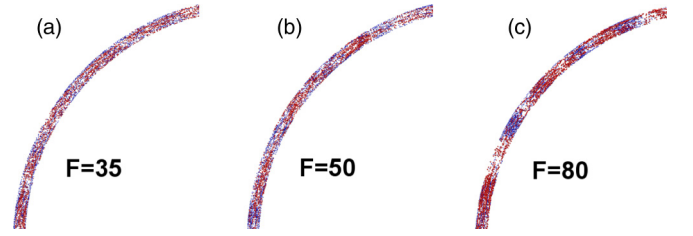


FIG. 3. Band formation in systems of inner radius $R_1 = 400$ with width $W = 20$ and force (a) $F = 35$, (b) $F = 50$, and (c) $F = 80$. In order to better recognize the particle distribution, a section of the ring was enlarged. The red particles move clockwise against the blue ones.

the channel the particles are evenly distributed. A band order parameter greater than 1 indicates that the local density in some bins is more than twice as high as the average density. The order parameter has a theoretical upper bound of $\Phi_{\text{band}} = n_{\text{bin}}$, due to the finite bin width. By evaluating the simulations by eye we chose the critical value of the band formation to be $\Phi_{\text{band}} = 0.25$ above which the system can be considered ordered. Analogously to lane formation, the critical force $F_{c,\text{band}}$ is defined as the force where the critical band formation parameter is reached.

IV. RESULTS

All results are given in units of the particle diameter σ , the unit of thermal energy kT , and the diffusion coefficient D_0 . All simulations were done at a fixed density $n_{\text{tot}} = 0.32$, and a fixed inverse screening length $\kappa = 3.0$. The interaction strength is solely regulated with the parameter V_0 . We chose $V_0 = 37.0$, which is similar to the interaction strength used in Refs. [13,30].

In Sec. IV A, we study the order with varying system sizes by increasing the inner radius from $R_1 = 10$ to $R_1 = 100$ with an increment of 10 and from $R_1 = 100$ to $R_1 = 600$ with an increment of 100. We also study four different widths $W = \{10, 20, 35, 50\}$.

For each system the driving force F is increased in steps of $\Delta F = 5$ in the interval $F \in [10, 85]$. The respective simulations for each force consist of 10^6 time steps at a step size of $\Delta t = 7.5 \times 10^{-5}$. To confirm that the given simulation length is sufficient for our statements we performed test simulations with a simulation time that was five times as long for four data points in Fig. 4(b) below of the small systems. The trends between the different systems stayed identical; only the critical forces showed a decrease of 5%–10%. A similar test was done for the big systems with twice the simulation length. Here the trends of the phase diagram in Fig. 11 below stayed identical as well. However, since the critical forces partially exhibited much larger deviations in these systems, we show none of these critical forces in this work. Therefore, we concluded the amount of simulation steps to sufficiently support our findings. The simulations are performed consecutively, which means that when a simulation is finished its final coordinates will be used as the starting coordinates of the next higher force. This process facilitates the formation of order and therefore reduces the simulation time.

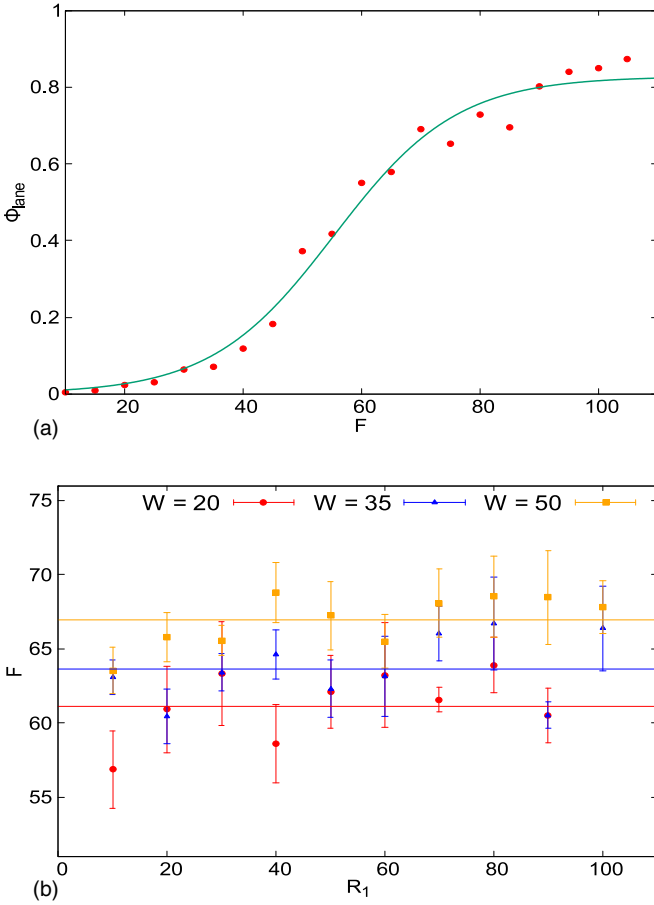


FIG. 4. (a) Order parameter Φ_{lane} in dependence on the force for the system size with $R_1 = 40$ and $W = 35$. This curve looks similar for all system sizes. For wider systems the curve flattens slightly, and the steep increase shifts to a higher value. (b) The critical force F_c of widths $W = 20$, $W = 35$, and $W = 50$ for all simulated radii up to $R_1 = 100$. The red circles correspond to systems of width $W = 20$, the blue triangles to systems of width $W = 35$, and the orange squares to systems of width $W = 50$. The average of all points is plotted with the three lines in their respective colors.

A. Order in small systems

Once a force is applied to both particle species, its order is formed in the system depending on the driving force F and the interaction strength V_0 . For small system sizes the well-known scenario of lane formation can be observed as it is known from linear channels in two dimensions [30] and three dimensions [13]. Figure 2 shows such systems for different driving forces F . In the regime of weak driving forces, the system is still disordered. Only locally particles of the same species move in small chains one behind the other. As soon as the force rises to a critical force however, the system starts to order itself. By further increasing the force, the particles separate into lanes spanning the full circle. This behavior can be found for all systems with an inner radius $R_1 \in [10, 200]$.

B. Order in big systems

In systems with inner radii $R_1 \geq 300$ a different kind of order phenomenon can be observed by increasing the driving

force. As shown in Fig. 3, the particles do not separate into lanes but form periodic bands perpendicular to the channel walls of the same particle species. In contrast to the jamming observed in the very narrow channels, the bands of different particle species interpenetrate and pass each other.

The bands have similar sizes and distances to each other but are still distinguishable. As a result of constantly losing and gaining particles while orbiting, the bands themselves, however, are not stable.

The number of bands depends on the radius and the width of the system. By looking at the mechanism how the bands form, we can recognize that the particles of the same species accumulate together. At first, density fluctuations of a certain length scale form, and as they pass through the channel, the particles keep together despite there being no attractive forces. The result of this accumulation is the formation of the bands.

Focusing on the regime of $F \in [35, 50]$ in the simulations in Fig. 3, we notice that the particles start to pile up and tear small gaps. These gaps increase with the increasing force.

Because of this phenomenon, further simulations with changed parameters were performed. For systems with inner radii $R_1 = 300$ and $R_1 = 400$ widths of $W = 20, 35$, and 50 were considered.

C. Order parameter for lane formation and critical force

The order parameter Φ_{lane} yields a numerical value between zero and unity. The critical force F_c is defined as the force at which the order parameter reaches the value $\Phi_{\text{lane}} = 0.5$.

This can be reasoned by comparing the behavior of the order parameter in Fig. 4(a) with the corresponding configurations in Fig. 2. We notice that the value of Φ_{lane} increases with the driving force and thus the order in the system increases as well. Furthermore we see that the order parameter Φ_{lane} begins to increase significantly with a driving force of $F = 30$ until it converges towards a value near unity at a force of about $F = 75$. For a force of $F = 60$ [Fig. 2(b)] the system is reasonably ordered, and the order parameter for the first time exceeds the value $\Phi_{\text{lane}} = 0.5$.

To extract the critical force the order parameter for each system is empirically fitted by the function

$$f(F) = \frac{1}{4}(\cos(a) + 1) \left[\tanh\left(\frac{F - c}{b}\right) + 1 \right].$$

The first term of the function sets the boundaries of the fit to stay in the range of $f(F) \in [0, 1]$, while the second term yields the sigmoidal shape of the fit. a , b , and c are fit parameters, and F is the driving force.

Figure 4(b) shows the critical force as a function of the inner radius in the range between $R_1 = 10$ and $R_1 = 100$ for three widths $W = 20, W = 35$, and $W = 50$. In this range the critical force does not depend on the length of the channel, which is determined by the inner radius, and only weakly on the width of the channel. For each data point 10 simulations with different starting positions were performed, and their respective critical forces F_c were averaged. Table I shows how many of these 10 simulations form lanes. It can be seen that for larger inner radii R_1 and a width of $W = 20$ only a few simulations form lanes (which is in line with Sec. IV F). The

TABLE I. Amount of lane forming simulations n_{lane} out of 10 different starting points. These data correspond to Fig. 4(b).

R_1	$W = 20$	$W = 35$	$W = 50$
10	9	8	9
20	9	10	10
30	9	10	10
40	4	10	10
50	7	10	10
60	4	9	10
70	7	8	9
80	3	8	10
90	3	6	9
100	2	6	7

data point corresponding to a system with an inner radius of $R_1 = 100$ and a width of $W = 20$ was omitted because a sample size of $n_{\text{lane}} = 2$ was considered too small. Due to the small width at $W = 10$ not all systems could arrange correctly. The influence of the hard walls as described in Sec. IV A is crucial. Therefore, the values with width $W = 10$ are missing in Fig. 4(b).

By averaging the critical force F_c over all systems with equal widths, the mean $\bar{F}_{c,20} = 61.1$ for $W = 20$, $\bar{F}_{c,35} = 63.6$ for $W = 35$, and $\bar{F}_{c,50} = 66.9$ for $W = 50$ can be determined, which results in differences of about $\Delta F_{c,20-35} = 2.5$ and $\Delta F_{c,35-50} = 3.3$.

From these data it seems that the lane formation survives for all channel lengths, since the critical force is constant with increasing the radius R_1 . But for larger systems the behavior suddenly changes. For systems with a larger inner radius band order occurs, which prevents the system from ordering in lanes. In the next section we want to answer the question how the occurrence of bands depends on the system parameters.

D. Varying the width and interaction strength

For the systems with an inner radius of $R_1 = 300$ and an interaction strength of $V_0 = 35$ we found band order for all widths $W = 20, 35$, and 50 . By increasing the interaction strength to $V_0 = 65$, the particles arrange themselves into lanes again as seen in the small systems in Fig. 5(b).

These results were determined by using the histograms in Sec. IVE and the order parameter Φ_{band} . The structures in Fig. 5 show which order exists and how many bands or layers arise during separation. Here the biggest driving forces are presented because the order of the particles is most pronounced there.

If we analyze the band order in Fig. 5(a), we see that the bands do not have the exact same sizes or the same distances between each other, but rather that they differ by slight amounts. With this graph the number of bands can be easily determined. The bands do not necessarily have the same size for the two particle species. For the systems with $R_1 = 300$ and $R_1 = 400$ the bands have widths of about 10° , which means they are slightly larger for the system with $R_1 = 400$. If we increase the channel width W in the system with $R_1 = 300$ and $V_0 = 35$, it can be seen that the number of bands decreases with the width of the system (see Fig. 6), whereas in the

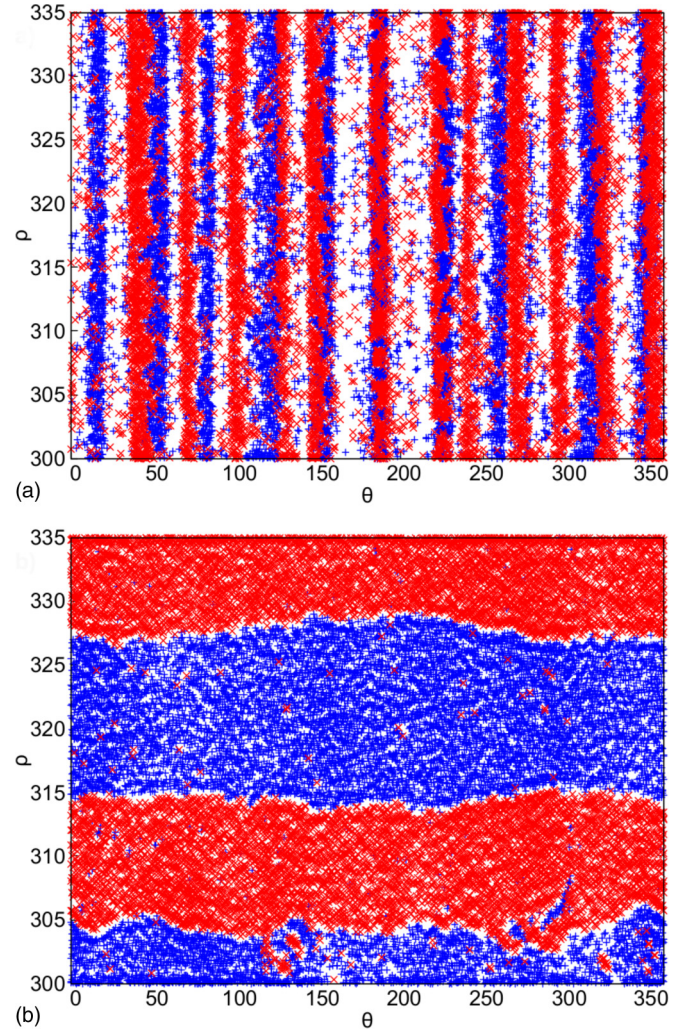


FIG. 5. Particle positions in the system with $R_1 = 300$, $W = 35$, (a) $V_0 = 35$, and (b) $V_0 = 65$ for the driving force $F = 85$. The graphic shows the position over the radius and the angular coordinate. Red shows the positions of the particles which are moved in a clockwise direction. The blue particles move counterclockwise. In panel (a) we see band order, whereas in panel (b) the particles break up into lanes.

system $R_1 = 300$ and $V_0 = 65$ the number of lanes increases with increasing width (see Fig. 7).

What can be detected for both systems at $V_0 = 35$ is that for widths of $W = 50$ the bands start smearing. This means that the band order and the order parameter Φ_{band} decreases.

If we look at the systems with $V_0 = 65$ in Fig. 7, we can see lane formation. With a radius of $R_1 = 300$ and a width of $W = 20$ three lanes are visible. If we increase the width to $W = 35$ another lane appears, and the same happens by increasing the width again to $W = 50$. Thus it can be said that the number of lanes increases with the system width. The width of the lanes W_{lane} themselves differs only slightly and is in the range $W_{\text{lane}} = 10$ and $W_{\text{lane}} = 12$. Narrower lanes are possible only at the edges of the system; this depends on the overall width of the system. The difference in the configurations for radii $R_1 = 300$ and $R_1 = 400$ is that the system with the larger radius and the same width has one lane less.

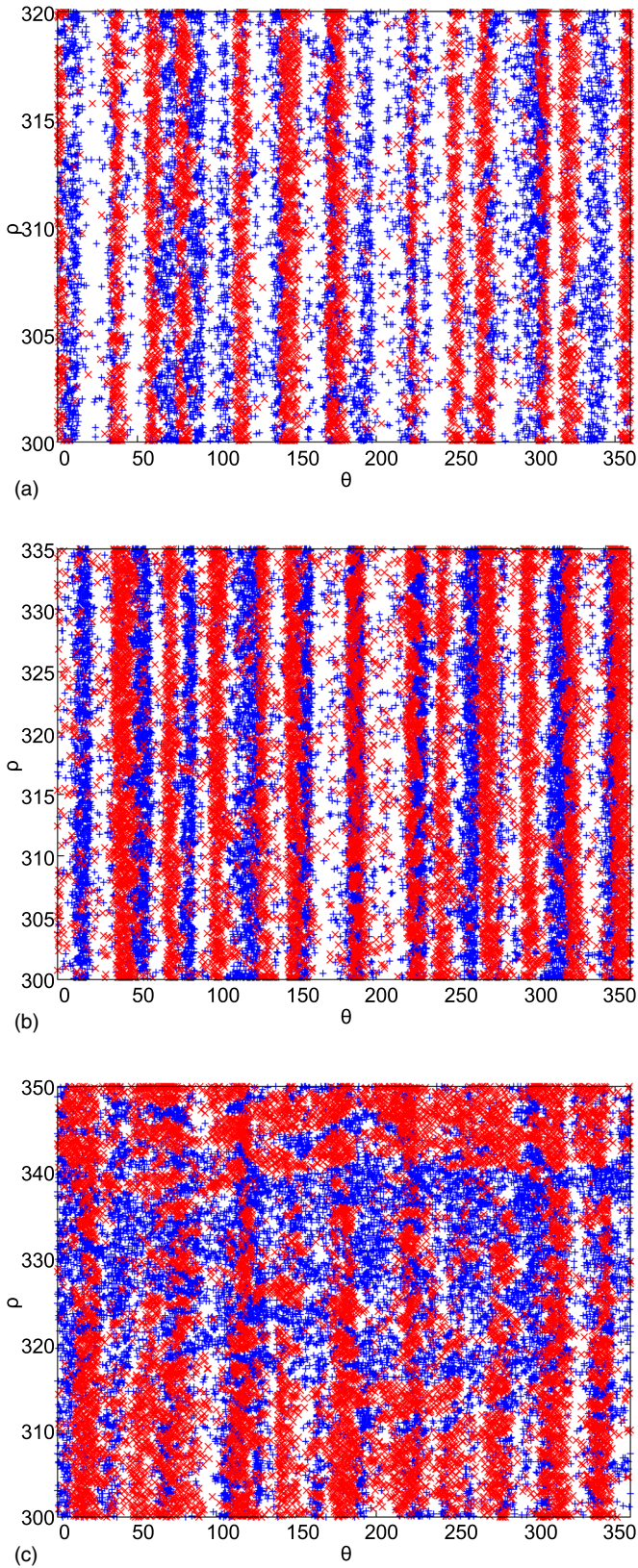


FIG. 6. Particle positions for the systems with $R_1 = 300$, $W = 20, 35, 50$ for $F = 85$ and an interaction strength of $V_0 = 35$. It can be seen that in this system size the number of bands decreases with increasing width. At a width of $W = 50$ the band order smears and the order parameter decreases.

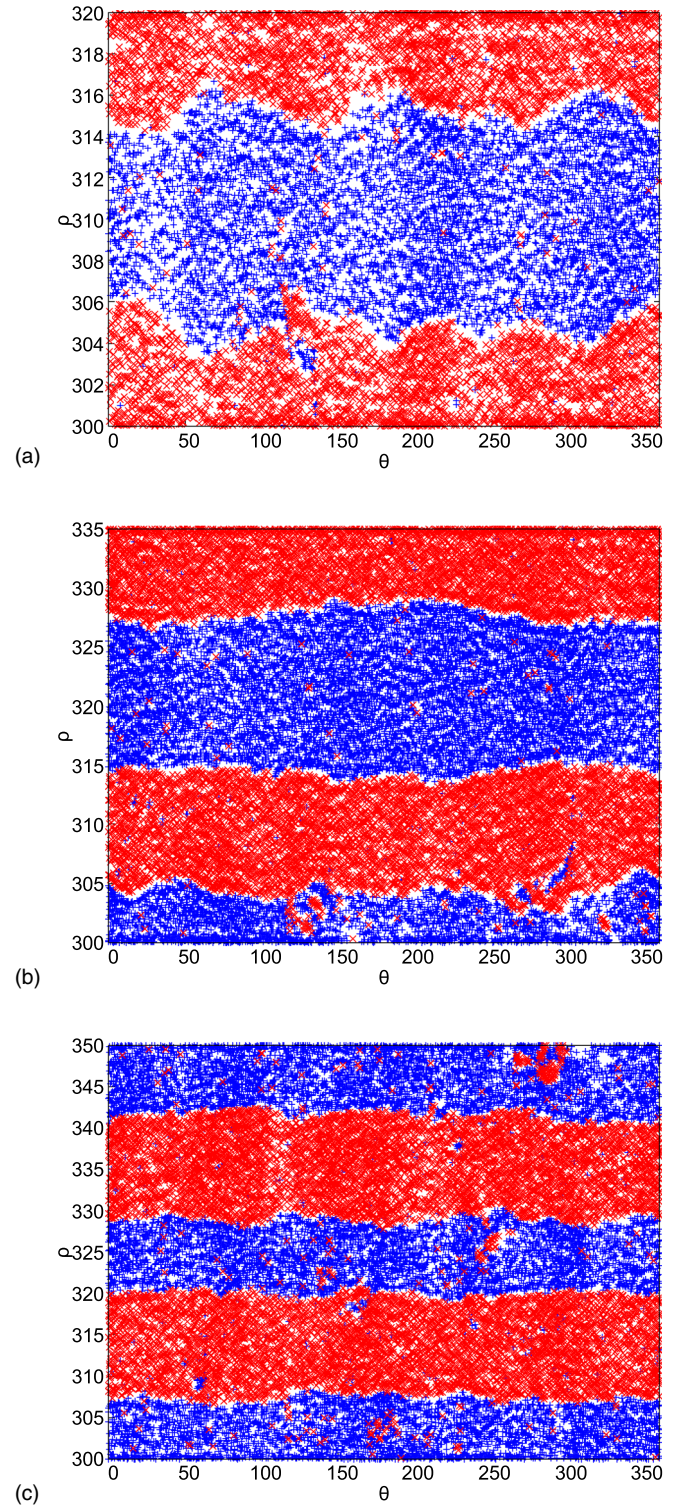


FIG. 7. Particle positions for the systems with (a) $W = 20$, (b) $W = 35$, and (c) $W = 50$, $R_1 = 300$ and an interaction strength of $V_0 = 65$ with a driving force of $F = 85$. The graphs show that by increasing the width of the system, for every step of $\Delta W = 15$ one additional lane is created.

Comparing our results of circular channels to those of linear channels we can see general accordance. References [13], [19], and [30] all showed a similar S-shaped increase of the

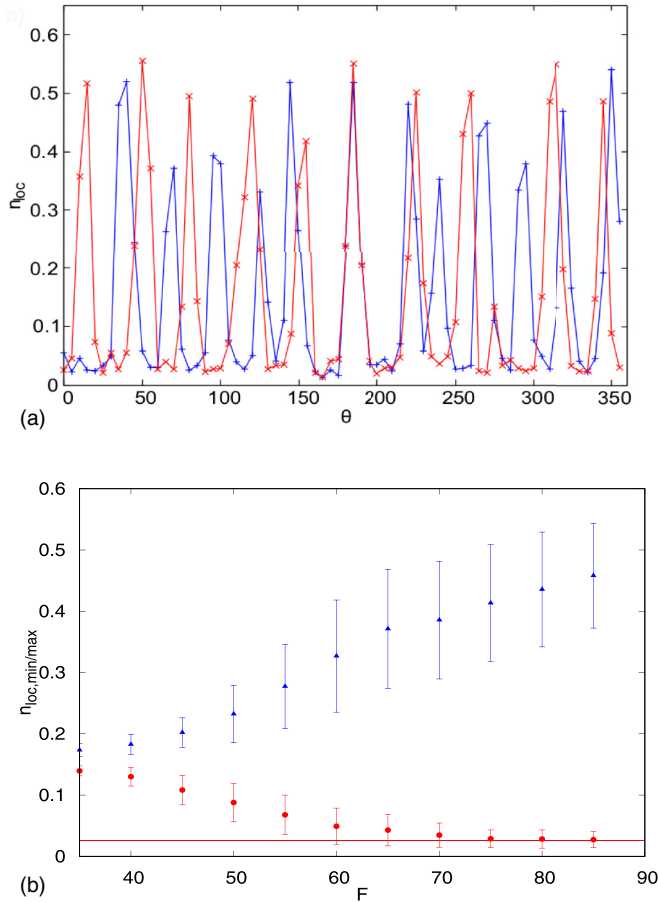


FIG. 8. (a) Local particle density n_{loc} plotted over the angular coordinate of the system $R_1 = 300$, $W = 35$, and $V_0 = 35$ for a snapshot at a driving force of $F = 85$. Here the two particle species are counted and plotted as the local density in a 5° interval. The density in the system is $n_{tot} = \frac{N}{A} = 0.32$. (b) Force dependence of the minimum and the maximum local particle density as a function of the driving force F . The minimum and maximum values are represented by the red circles and the blue triangles, respectively. A high maximum value implies the existence of dense cluster, whereas a low minimum value means that there are gaps in the system.

lane formation order parameter with an increase in force. The 3D systems from Ref. [13] with hard walls exhibited only two particle regions, while the 2D and 3D systems from Ref. [19] with periodic boundaries, and the 2D systems from Ref. [30] all showed the emergence of multiple lanes. A potential difference, however, can be found in the dependence of the critical force on the system sizes. While in the circular channels we see an increase of the critical force only with an increase of the channel width, the linear channels in Ref. [30] show a logarithmic dependence of the critical force on the total system size. It is, however, also possible that the increase in the linear channels depends only on the channel width, which would mean that these results show accordance as well.

E. Order parameter for band formation

In order to determine the order parameter Φ_{band} the variance of the particle distribution is considered first. Figure 8(a)

shows the local density plotted over the angular coordinate, whereby the two particle species are considered separately. The local density for the same type of particles is summed up and plotted every five degrees. For the band order a large variance is observed. This means that we see big jumps in the curve of Fig. 8. In the areas where a band is located the number of particles is very high, whereas the number of particles in the region of a gap is very low. Figure 8(a) also confirms that the size and the distance of the bands vary. At an angular coordinate of 180° , two oppositely driven bands pass through each other. At this point it comes to the impoundment.

It is clearly visible that there is a nonzero density in the gaps. Figure 8 shows that the minimum density is roughly the same for all gaps and for both particle species. A value for the minimum and maximum density of the system can be extracted by averaging over all local minima, with a density which is smaller than the mean density, and over all local maxima, with a density which is higher than the mean density.

For the simulation, for which the local density is plotted in Fig. 8(a), the density in the gaps is $n_{loc, min} = 0.026$. The dense bands have a peak density between $n_{loc} = 0.3$ and $n_{loc} = 0.55$, but the big variance in the peak density is probably more due to the finite bin size and dissolving bands. The average over the maxima gives an estimation for the density of the bands of $n_{loc, max} = 0.46$.

Figure 8(b) shows these minimum and maximum densities as a function of the force F . It shows that while the minimum density converges to a finite value, the maximum density grows further by increasing the force. We therefore have a microphase separation of a phase of a high and one of a low particle density.

As described in Sec. III, the order parameter Φ_{band} is determined in terms of roughness of the local particle density. Figure 9(a) shows the order parameter Φ_{band} for the system with $R_1 = 300$, $W = 35$, and $V_0 = 35$, which orders in bands. The order parameter grows with increasing driving force. In the range of the critical force $F_c = 53.2$ it increases strongly, flattens again at $F = 75$, and finally converges to a value of $\Phi_{band} \approx 1.2$. The order parameter Φ_{band} has a similar S-shape progression as the order parameter Φ_{lane} for small systems. Up to a threshold force of $F = 35$ the system is basically disordered. Only if the force is further increased does the system start to order. At the point of $F = 50$, band order can be detected with the order parameter Φ_{band} . By comparing the big system with the small system, it turns out that the critical force for band formation of between $F_c = 50$ and 55 is smaller by 10 than the critical force for lane formation in the small system. This suggests that formation of bands in the big system prevents the formation of lanes which would occur only for higher forces.

Figure 9(b) shows the number of bands as a function of external force, where a band is counted if the local density grows by more than a threshold value of $\Delta n_{loc} = 0.08$. The number of bands is averaged over both species and all time steps. The number of bands grows rapidly by increasing the force over $F = 50$, and then stays at a constant value, which in this system is $N_{band} \approx 13$. This is in contrast to the behavior of the order parameter, which grows further.

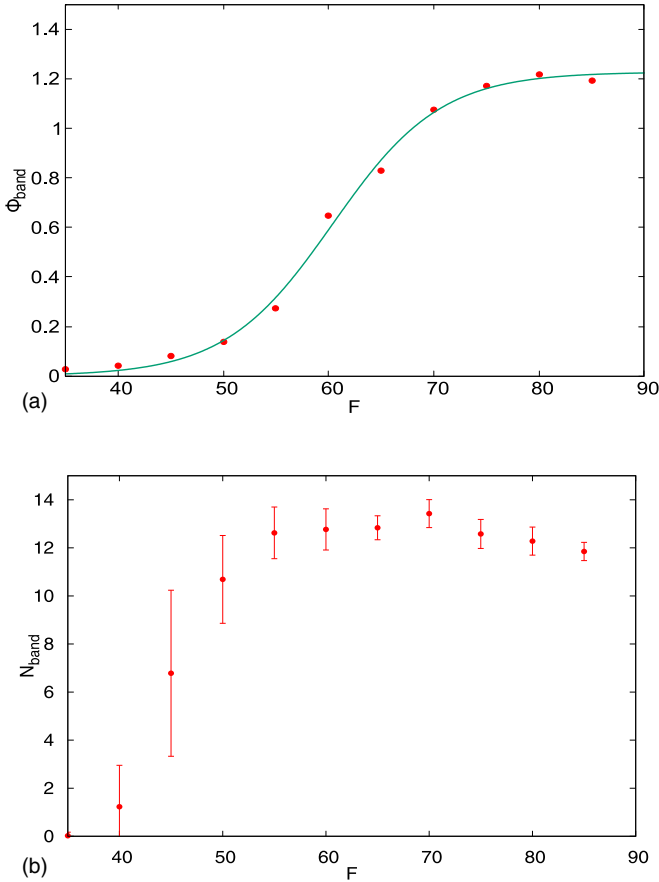


FIG. 9. (a) The order parameter for band formation Φ_{band} as a function of the driving force for the system with inner radius $R_1 = 300$, width $W = 35$, and potential strength $V_0 = 35$. The critical force is defined at the point where $\Phi_{\text{band}} = 0.25$ is extracted from the fit. In this case the critical force is $F_c = 53.4 \pm 0.67$. (b) The number of bands N_{band} of one particle type as a function of the driving force for the specified parameters. A band is counted if there is an increase of the local density of $\Delta n_{\text{loc}} = 0.08$.

F. Transition from band formation to lane formation

In this section we show in which parameter range the transition of band formation to lane formation takes place in order to be able to restrict the occurring band order to a certain area. To find such a range, the channel width W of the system sizes with a radius of $R_1 = 300$ was increased in steps of $\Delta W = 5$ in a range of $W = 20$ to $W = 50$. For each of these systems, simulations with potential strengths from $V_0 = 35$ to $V_0 = 65$ were performed in increments of $\Delta V_0 = 3$. Figure 10 shows a simulation in which the two orders can be recognized. For values of the potential strength in the range of $V_0 = 50$ and $F = 60$, there is an overlap of band formation and lane formation. By increasing the driving force F the system will switch into one of the two orders.

If we compare the two order parameters Φ_{band} and Φ_{lane} for a system in which both bands and lanes exist [Figs. 10(b) and 10(c)], we see that both order parameters are close to their critical value. Φ_{band} and Φ_{lane} increase up to a critical force of $F_c = 65$ and converge to a value from there. These values are $\Phi_{\text{band}} = 0.23$ and $\Phi_{\text{lane}} = 0.48$. Thus both orders

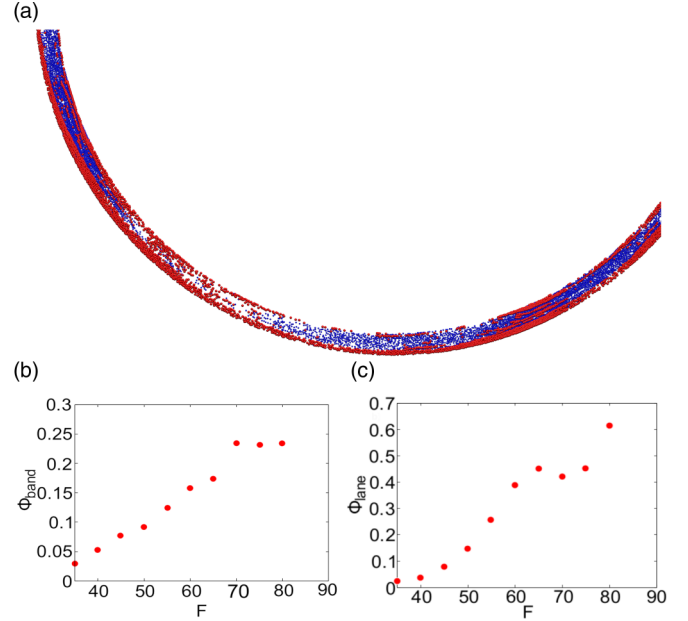


FIG. 10. (a) A system with $R_1 = 400$, width $W = 25$ and potential strength $V_0 = 59$, and a driving force of $F = 60$. This system is transitioning from band formation to lane formation. Evident are the lanes of the two particle types and at the same time accumulations of particles distributed in the ring. The comparison of the two order parameters for (b) band and (c) lane formation shows that in this system both orders exist.

are visible in the simulation. The value of the parameters shows that neither lane nor band formation outweighs the other. Only with a driving force of $F = 80$ does the order parameter Φ_{lane} exceed its critical value of 0.5, while the band parameter remains at $\Phi_{\text{band}} = 0.23$. If we consider this system for larger potential strengths the system orders in lanes, and if we reduce the potential strength, band formation would occur.

For precise statements a statistical analysis was performed to get a probability distribution; see Fig. 11. This graph shows the distribution of all systems with radius $R_1 = 300$. Due to the large system size and their computing time, five simulations with different starting positions were carried out for each parameter combination in a force range of $F \in [30, 85]$ and a step size of $\Delta F = 5$. The probability P is calculated by examining the system for its order at the highest driving force. If we observe band formation, unity is added, and if there is lane formation, unity is subtracted from a counter. This counter is then divided by five, and we get a value between $P = 1$ equaling 100% band formation and $P = -1$ equaling 100% lane formation.

If we look at Fig. 11, we can see that for systems with small width $W = 20$ and small potential strength $V_0 = 35$ there is a 100% probability for band formation, whereas for large width of $W = 50$ and high potential strength $V_0 = 65$ lane formation is found with a 100% probability. The probability distribution shows that both the width and potential strength influence the order in the system. If we investigate systems with a constant width of $W = 20$ by increasing the potential strength, the probability for lane formation increases. Similarly, the

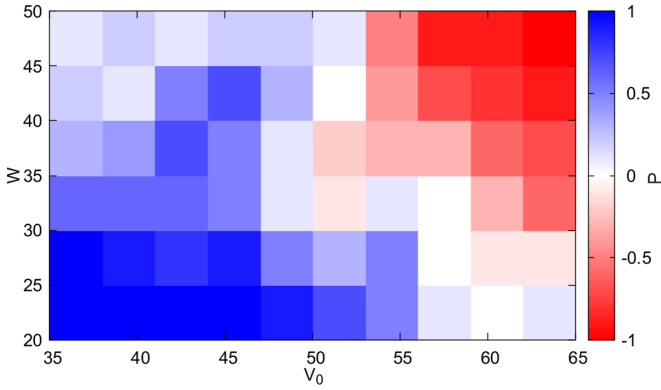


FIG. 11. Probability to find the system in the ordered state with band or lane formation for all systems with inner radius $R_1 = 300$. The probability depending on the width W and potential strength V_0 of the system. A value of $P = 1$ (blue) represents 100% band formation, and $P = -1$ (red) represents 100% lane formation. For small widths W and small potential strengths V_0 , band formation predominates. In systems with larger width and higher potential strength, lane formation is found.

probability for lane formation increases by increasing the width at constant strength of $V_0 = 35$.

In the area of the white fields in Fig. 11 the transition from band formation to lane formation takes place, where both types of order have the same probability. For example, in the system characterized by $W = 30$ and $V_0 = 57$, it is impossible to decide into which order the system will pass before the simulation is finished.

The phase diagram (Fig. 11) reflects the phenomenon of crossover from lane formation to band formation that we have already seen in examining the width and interaction strength for large radii in Sec. IV D. Figure 6(c) shows the system with a small potential strength $V_0 = 35$ and large width $W = 50$. It can be seen that the order of the band formation decreases in comparison to smaller widths of this system. In this case, such a crossover from band formation to lane formation can be recognized. Also Fig. 7(a) matches the scheme shown in Fig. 11; by looking at the areas of $\theta = 80$, 200, and 320, a higher local density is found. There the system with a higher potential strength $V_0 = 65$ and a small width $W = 20$ is described.

Comparing these results to Refs. [26] and [31] one can clearly see the novelty of band formation with a static rather than an oscillating driving force. Furthermore, in the linear 3D channels with hard walls in Ref. [13] longitudinal demixing was observed, an order formation similar to band formation with only two particle fronts, and therefore no periodicity. This phenomenon occurred only starting from high channel lengths and in thin channels, which compares well to the high radius R_1 and small channel width W necessary in the 2D circular channels. To check whether the dimensionality or the shape of the channel is crucial in the formation of the band structure, a simulation in a linear channel with hard walls parallel to the drive direction (x direction) was performed. The simulation was run with a potential strength of $V_0 = 35$, a channel width (y length) of $W = 25$, and a channel length (x length) of $L = 3000$, and periodic boundary conditions were

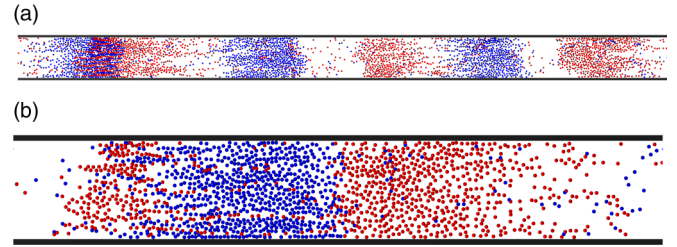


FIG. 12. (a) Snapshot of a simulation in a linear channel. The channel has a length of $L = 3000$ and a width of $W = 25$, and the potential strength was set to $V_0 = 35$. Since the channel is very long and rather thin, only a segment is shown here. The phenomenon of band formation can be clearly seen, and the bands also occur in the whole channel. (b) Closeup of two bands penetrating each other. To the left one can see a small red band that has almost completely passed through the blue band already, and to the right one can see the two fronts of different species hitting each other.

employed in the drive direction (x direction). These values were selected because we found band formation in exactly this parameter region in circular channels (see Fig. 11). Snapshots of this simulation are shown in Fig. 12 in which we can also clearly observe band formation. With these data one can conclude that the shape of the channel plays no role in whether or not bands can form. We also assume that the fact whether the systems are in two or three dimensions plays a crucial role in the formation of periodic band structures, as well as the confinement of the system.

To answer the question whether both ordering phenomena can be considered true phases with a phase transition, the thermodynamic limit with particle number $N \rightarrow \infty$ and area $A \rightarrow \infty$ has to be examined. The result will probably differ when the circular area is increased by either just increasing the radius $R \rightarrow \infty$ at constant channel width W or by increasing both, for example, with a constant ratio $W/R \leq 1$. It is furthermore unclear whether the dynamic system will then still reach its steady state within a finite time frame. These substantial aspects need further studies which are outside of the scope of this work.

V. CONCLUSION

In this work we showed that in two-dimensional circular channels of colloidal particles two kinds of dynamic order phenomena can be found by driving half of the particles clockwise and the other half counterclockwise: Either the lane formation transition occurs or a formation, of bands can be observed, depending on the control parameters.

For small systems with a radius of up to $R_1 \leq 200$, mostly lanes can be seen when increasing the driving force. The particles separate from each other by forming lanes. Thus the particles can move in opposite direction without encountering each other. These lanes are of approximately equal width. Therefore more and more lanes are created by increasing the width of the channel. The effect of hard walls can be noticed in channels with very small widths ($W \leq 10$) in which the ordering phenomena are disturbed. To quantify the order and to determine a critical driving force F_c at which the transition to lanes starts, the order parameter Φ_{lane} was introduced. The

critical force for lane formation was defined as the force where the order parameter exceeds the value $\Phi_{\text{lane}} = 0.5$ and was extracted by a fit. The critical force F_c of lane formation is in the range of $F_c = 62$ for narrower and $F_c = 67$ for wider circular channels. It increases slowly with the width of the channel, but seems to be nearly independent of the length of the channel, which is determined by the inner radius R_1 .

For systems with radii larger than $R_1 \geq 300$ and certain sets of parameters, the formation of bands of particles occurs. The bands consist of the same particles species, are oriented orthogonal to the driving force, and have a regular pattern. Such a band formation is known from oppositely charged colloidal particles with alternating electrical fields. A similar behavior of demixing of the two particle species is also recognized in three-dimensional channels [13], but there the particles form only two blocks of particles. Furthermore the formation of bands is also known from the Vicsek model. In our system the band formation is unexpected since the bands of different particle species have to regularly encounter each other.

The band formation can be interpreted as a micro phase separation of two coexisting phases. As can be seen from the plot of the local density as a function of the angular coordinate, the gaps have a small but finite constant density, and the bands have also a nearly constant density, which is introduced by the external driving force.

In large systems with a small interaction strength of $V_0 = 35$ the particles begin to accumulate in bands with gaps in between. The critical force for band formation, where the order parameter exceeds the critical value of $\Phi_{\text{band}} = 0.25$, was determined to be between $F_c = 52$ and $F_c = 55$, depending on the width of the channel. Thus the critical force for band formation is smaller than the critical force for lane formation. It is noticeable that at widths of $W = 50$, the particles begin to lose order and the order parameter decreases.

In large systems with a large interaction strength of $V_0 = 65$ we found significantly more frequent lane formation than band formation. Interestingly, the order of the particles depends not only on the radius of the system or the driving force but also the width W and the potential strength V_0 . Here the critical force is also in an area of approximately $F_c = 63$ for

lane formation and $F_c = 53$ for band formation. Interestingly, for larger widths and potential strength $V_0 = 65$, more lanes form. If we increase the width of the circular channel by 15 units, one additional lane was formed.

We varied these quantities of width W and potential strength V_0 for a fixed radius $R_1 = 300$ to explore a broader parameter range. A phase diagram depending on these two parameters is given by the probability distribution that band formation or lane formation is found. In order to obtain the probability distribution, several simulations with the same parameter combinations but different start positions were carried out.

In systems of small width and potential strength in 100% of the simulations band formation occurred. In the systems with large width and large potential strength, however, lane formation occurred in 100% of the simulations. The transition line from lane to band formation thus proceeds diagonally in the W, V_0 phase space.

As future work these parameter ranges could be examined in smaller systems with $R_1 \leq 200$. Furthermore it seems worthwhile exploring the influence of hydrodynamic interactions on band formation to model more realistic colloidal systems. In further studies hysteresis and bifurcation phenomena should also be examined, since it seems that in some configurations both orderings are stable depending on the starting condition. It would also be very interesting to explore systems with particles that are driven in the same direction to see whether new experimental systems could be created that use this kind of setup. Additionally, a closer look could be given at the formation and stability of the bands and lanes that form in these systems.

ACKNOWLEDGMENTS

This research was funded by the Deutsche Forschungsgemeinschaft DFG (Project No. NI259/16-1 and 299102402). The authors gratefully acknowledge the Gauss Centre for Supercomputing e.V. [40] for funding this project by providing computing time through the John von Neumann Institute for Computing (NIC) on the GCS Supercomputer JUWELS at Jülich Supercomputing Centre (JSC).

-
- [1] R. Haghgooe and P. S. Doyle, *Phys. Rev. E* **70**, 061408 (2004).
 - [2] P. Henseler, A. Erbe, M. Köppl, P. Leiderer, and P. Nielaba, *Phys. Rev. E* **81**, 041402 (2010).
 - [3] U. Siems, C. Kreuter, A. Erbe, N. Schwierz, S. Sengupta, P. Leiderer, and P. Nielaba, *Sci. Rep.* **2**, 1015 (2012).
 - [4] D. Wilms, N. B. Wilding, and K. Binder, *Phys. Rev. E* **85**, 056703 (2012).
 - [5] U. Siems and P. Nielaba, *Phys. Rev. E* **98**, 032127 (2018).
 - [6] M. Dreher, F. Pauly, J. Heurich, J. C. Cuevas, E. Scheer, and P. Nielaba, *Phys. Rev. B* **72**, 075435 (2005).
 - [7] F. Pauly, J. K. Viljas, M. Bürkle, M. Dreher, P. Nielaba, and J. C. Cuevas, *Phys. Rev. B* **84**, 195420 (2011).
 - [8] T. M. Squires and S. R. Quake, *Rev. Mod. Phys.* **77**, 977 (2005).
 - [9] B. Zhang and M. Radisic, *Lab Chip* **17**, 2395 (2017).
 - [10] I. D. Couzin and N. R. Franks, *Proc. R. Soc. Lond. B* **270**, 139 (2003).
 - [11] T. Bohlein, J. Mikhael, and C. Bechinger, *Nat. Mater.* **11**, 126 (2012).
 - [12] U. Siems and P. Nielaba, *Phys. Rev. E* **91**, 022313 (2015).
 - [13] B. Heinze, U. Siems, and P. Nielaba, *Phys. Rev. E* **92**, 012323 (2015).
 - [14] S. R. Nagel, *Rev. Mod. Phys.* **89**, 025002 (2017).
 - [15] J. Berner, B. Müller, J. Gomez-Solano, M. Krüger, and C. Bechinger, *Nat. Commun.* **9**, 999 (2018).
 - [16] T. Brazda, A. Silva, N. Manini, A. Vanossi, R. Guerra, E. Tosatti, and C. Bechinger, *Phys. Rev. X* **8**, 011050 (2018).
 - [17] J. M. Pagès, A. V. Straube, P. Tierno, J. Ignés-Mullol, and F. Sagués, [arXiv:1806.09913](https://arxiv.org/abs/1806.09913).

- [18] J. Olarte-Plata, J. M. Rubi, and F. Bresme, *Phys. Rev. E* **97**, 052607 (2018).
- [19] J. Dzubiella, G. P. Hoffmann, and H. Löwen, *Phys. Rev. E* **65**, 021402 (2002).
- [20] C. Reichhardt, J. Thibault, S. Papanikolaou, and C. J. O. Reichhardt, *Phys. Rev. E* **98**, 022603 (2018).
- [21] D. Helbing, L. Buzna, A. Johansson, and T. Werner, *Transp. Sci.* **39**, 1 (2005).
- [22] M. Moussaid, D. Helbing, and G. Theraulaz, *Proc. Natl. Acad. Sci. USA* **108**, 6884 (2011).
- [23] J. Lee, T. Kim, J.-H. Chung, and J. Kim, *KSCE. J. Civ. Eng.* **20**, 1099 (2016).
- [24] M. E. Leunissen, C. G. Christova, A.-P. Hynninen, C. P. Royall, A. I. Campbell, A. Imhof, M. Dijkstra, R. van Roij, and A. van Blaaderen, *Nature (London)* **437**, 235 (2005).
- [25] T. Vissers, A. Wysocki, M. Rex, H. Loewen, C. P. Royall, A. Imhof, and A. van Blaaderen, *Soft Matter* **7**, 2352 (2011).
- [26] T. Vissers, A. van Blaaderen, and A. Imhof, *Phys. Rev. Lett.* **106**, 228303 (2011).
- [27] K. R. Sutterlin, A. Wysocki, A. V. Ivlev, C. Raeth, H. M. Thomas, M. Rubin-Zuzic, W. J. Goedheer, V. E. Fortov, A. M. Lipaev, V. I. Molotkov *et al.*, *Phys. Rev. Lett.* **102**, 085003 (2009).
- [28] M. Rex and H. Löwen, *Phys. Rev. E* **75**, 051402 (2007).
- [29] M. Rex and H. Löwen, *Eur. Phys. J. E* **26**, 143 (2008).
- [30] T. Glanz and H. Löwen, *J. Phys.: Condens. Matter* **24**, 464114 (2012).
- [31] A. Wysocki and H. Löwen, *Phys. Rev. E* **79**, 041408 (2009).
- [32] T. Vicsek, A. Czirók, E. Ben-Jacob, I. Cohen, and O. Shochet, *Phys. Rev. Lett.* **75**, 1226 (1995).
- [33] G. Grégoire and H. Chaté, *Phys. Rev. Lett.* **92**, 025702 (2004).
- [34] A. P. Solon, H. Chaté, and J. Tailleur, *Phys. Rev. Lett.* **114**, 068101 (2015).
- [35] A. Wysocki and H. Löwen, *J. Phys.: Condens. Matter* **23**, 284117 (2011).
- [36] J. Bleibel, A. Domínguez, F. Günther, J. Harting, and M. Oettel, *Soft Matter* **10**, 2945 (2014).
- [37] D. L. Ermak and Y. Yeh, *Chem. Phys. Lett.* **24**, 243 (1974).
- [38] T. Glanz, R. Wittkowski, and H. Löwen, *Phys. Rev. E* **94**, 052606 (2016).
- [39] H. Behringer and R. Eichhorn, *Phys. Rev. E* **83**, 065701(R) (2011).
- [40] Gauss Centre for Supercomputing e.V., www.gauss-centre.eu.